

# Macro- and micro-mechanical characteristics of crushed rock aggregate subjected to direct shearing



Jiankun Liu<sup>\*</sup>, Pengcheng Wang, Jingyu Liu

Department of Civil Engineering, Beijing Jiaotong University, Beijing 100044, China

## ARTICLE INFO

### Article history:

Received 2 December 2013

Revised 17 June 2014

Accepted 30 July 2014

Available online 10 August 2014

### Keywords:

Crushed rock aggregate

Large-scale direct shear test

Particle flow model

Mechanical behavior

## ABSTRACT

To study the mechanical behavior of crushed rock aggregate, a series of large-scale direct shear tests were conducted. Then the particle flow model was established with PFC3D (Particle Flow Code 3D) to analyze the micro-mechanical properties, including the distribution of contact forces and displacement vectors. The clump logic was adopted to replace the spheres to simulate the irregular particle. The main results were: The shear strength of crushed rock aggregate increased obviously with the increase of normal stress, and a strength envelope of the power function type was suitable for assessing this; within the range of chosen normal stresses, volumetric dilation was always observed after compression, and smaller normal stress led to larger dilation as well as a less amount of compression; within certain particle sizes, the shear strength at the same normal stress and compression displacement increased with increasing particle size, while the apparent friction angle showed an opposite trend; and the formation of the shear band and evolution of the volumetric strain were elucidated.

© 2014 Elsevier Ltd. All rights reserved.

## Introduction

Crushed rock aggregate is widely used as railway ballast and embankment filling in civil engineering. In permafrost regions, crushed rock subgrade has been used to cool the basement, which can be divided into crushed rock cushion subgrade, rubble slope subgrade, and U-type gravel subgrade laying crushed rock both on the slope and the bottom of the subgrade (Mu et al., 2010), as shown in Fig. 1. Crushed rock subgrade, which is also called “air convection embankment” (Saboundjian and Goering, 2003) has been proved to be an effective way to adjust the temperature field in subgrade due to its natural convection cooling ability (Goering and Kumar, 1996; Goering, 2003; Cheng, 2005). Intensive studies have been performed, both experimentally and theoretically, on the cooling effect of crushed rock subgrade, such as trying to determine the

optimal gravel size and laying position (Lai et al., 2003, 2004; Wu et al., 2005; Ma et al., 2008), but few studies on the mechanical properties of the loose and porous aggregate can be found, which can significantly affect the stability of subgrade, considering the long-term cyclic vehicle loads and harsh environments in cold regions.

Currently, there is no agreement on the optimal gravel size of crushed rock subgrade. However, in order to ensure a good cooling effect, large gravel size has been generally adopted, but this may reduce the stability of the subgrade. Large-scale tests are difficult to implement compared with conventional laboratory tests and numerical simulation. Considering the cohesionless characteristics of large-sized crushed rock, the discrete element method (DEM) has been proved to be efficient. The commercial software Particle Flow Code (PFC; Itasca Consulting Group, Minneapolis, MN, USA) has been widely applied in geotechnical engineering (Zhou and Jia, 2008). Wee (2004) simulated crushing tests and compression tests of ballast with PFC3D and analyzed the changes in mechanical properties of the

<sup>\*</sup> Corresponding author.

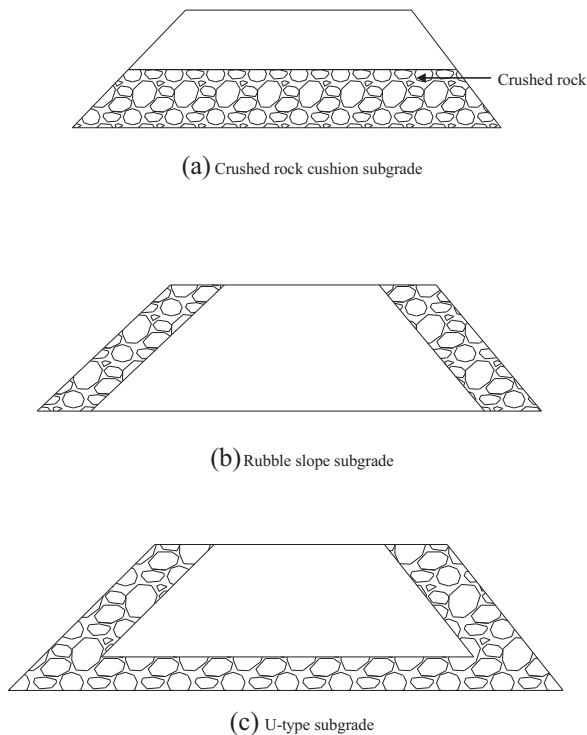


Fig. 1. Crushed rock subgrade of different types.

ballast. Indraratna et al. (2014) established direct shear test conditions by PFC3D and studied the changes in the mechanical properties of fresh and fouled ballast, and their results showed that the numerical results agreed well with the experimental results. Shao et al. (2013) simulated a large triaxial test of rock fill in drained shear conditions with the particle flow method.

In this paper, a large direct shear apparatus was used to study the mechanical properties of crushed rock aggregate of different sizes, and a DEM model was established with PFC3D to study the micro-mechanical characteristics during shearing, the model parameters were calibrated



Fig. 2. Large-scale direct shear apparatus at Beijing Jiaotong University.

**Table 1**  
Gradation selected in the tests.

Gradation	Particle size (cm)
A	2.5–3.5
B	3.5–4.5
C	4.5–5.5

by comparing the numerical results with experimental results.

## Laboratory experimental program

### Testing apparatus

The large-scale, strain-controlled direct shear apparatus (Fig. 2) developed by Beijing Jiaotong University was adopted to perform the lab tests. The sizes of the upper shear box and lower shear box were the same (30 cm × 30 cm × 10 cm). The upper box was pushed horizontally with a fixed lower box at a specific rate to complete the shearing process. The servo control system was used to apply the load and collect data automatically.

### Materials tested

All the aggregate tested was granite which was taken from a typical crushed rock subgrade section of the Qinghai-Tibet Railway. Following Indraratna et al. (1993), the size of the test equipment should be at least seven times larger than the majority of particles to eliminate the size effect. The grain gradation in the crushed rock subgrade was uniform to ensure the cooling effect, and three typical gravel sizes selected in this research are shown in Table 1.

To prepare the specimen, the aggregate was loaded into the shear box by lifts before being compacted to the specific dry density of 1.5 g/cm<sup>3</sup>. The specimen was first subjected to selected normal stresses (50 kPa, 100 kPa, 150 kPa, and 200 kPa) after compaction, and then it was sheared by pushing the upper box at the rate of 2 mm/min.

## Laboratory experimental test results

### Strength characteristics

The obtained strength properties of crushed rock aggregate are shown in Fig. 3. With the increasing vertical pressure, the shear strengths of all the gravel sizes clearly increased during shearing. The shear strain and shear stress curves basically show the characteristics of strain softening, where each curve has obvious fluctuation. The larger the vertical pressure and particle sizes, the more obvious the fluctuation, as expected, which was mainly due to breakage.

Tian et al. (2005) proposed that the strength envelope of rock fill is nonlinear; based on which, the relationship between shear strength ( $\tau_f$ ) and vertical pressure ( $\sigma_n$ ) is plotted in Fig. 4. As the particle size gets larger, the shear strength at the same vertical pressure increases. The effect

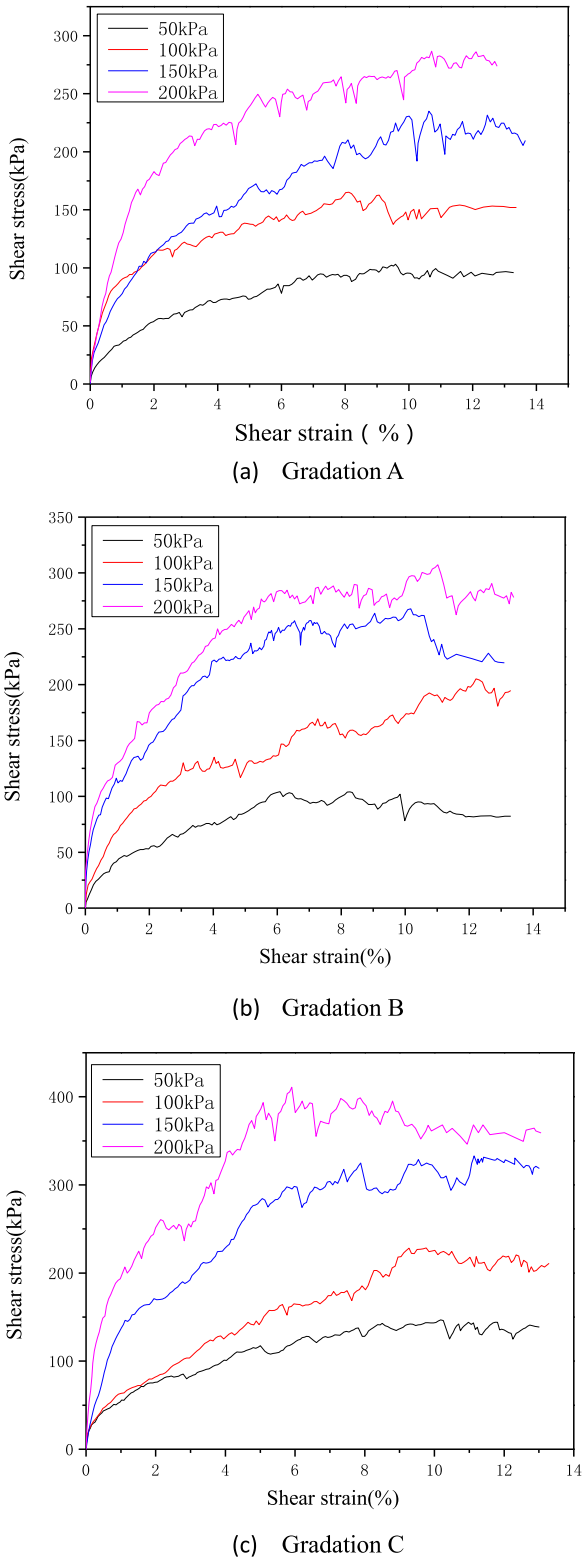


Fig. 3. Shear strain–stress curves of different particle sizes.

of particle size is more obvious with the increase of vertical pressure.

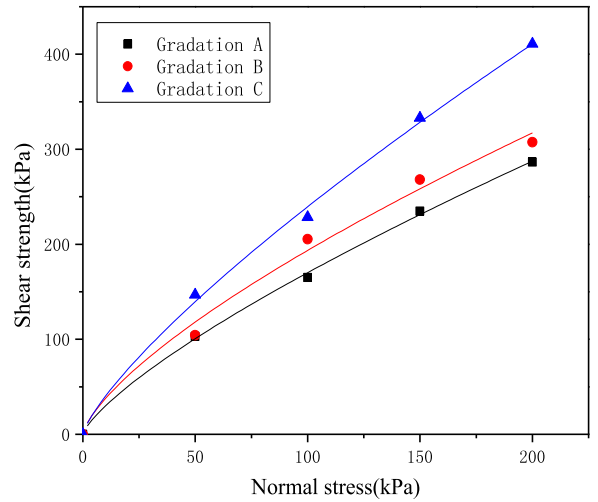


Fig. 4. Strength envelopes of different particle sizes.

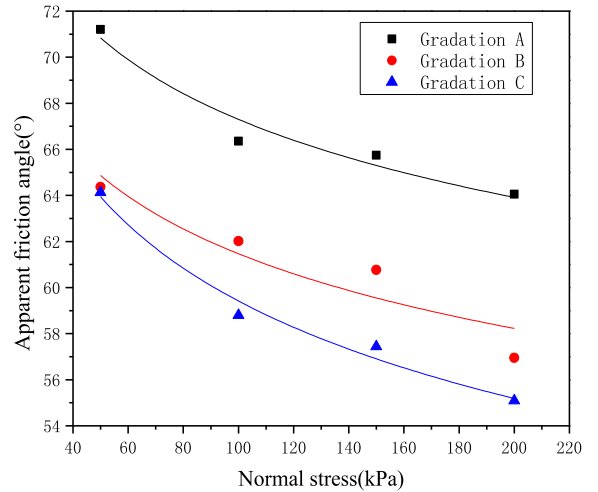


Fig. 5. Apparent friction angle.

A power function can be used to fit the strength envelope, and the equations are as follows:

$$\begin{cases} \tau_f = 5.211\sigma_n^{0.757}, & R^2 = 0.996, & 2.5\text{--}3.5 \text{ cm} \\ \tau_f = 7.274\sigma_n^{0.713}, & R^2 = 0.967, & 3.5\text{--}4.5 \text{ cm} \\ \tau_f = 6.654\sigma_n^{0.778}, & R^2 = 0.993, & 4.5\text{--}5.5 \text{ cm} \end{cases} \quad (1)$$

Indraratna et al. (1998) proposed the concept of apparent friction angle (a tangent from the origin to each Mohr circle of effective stress) in order to describe the change of the friction angle with the nonlinear variation of shear strength. Based on this, the apparent friction angles of different particle sizes under different pressure conditions were calculated and the curve fitting is shown in Fig. 5.

The apparent friction angle of the gravel decreased with increasing vertical pressure and gravel size. The greater the

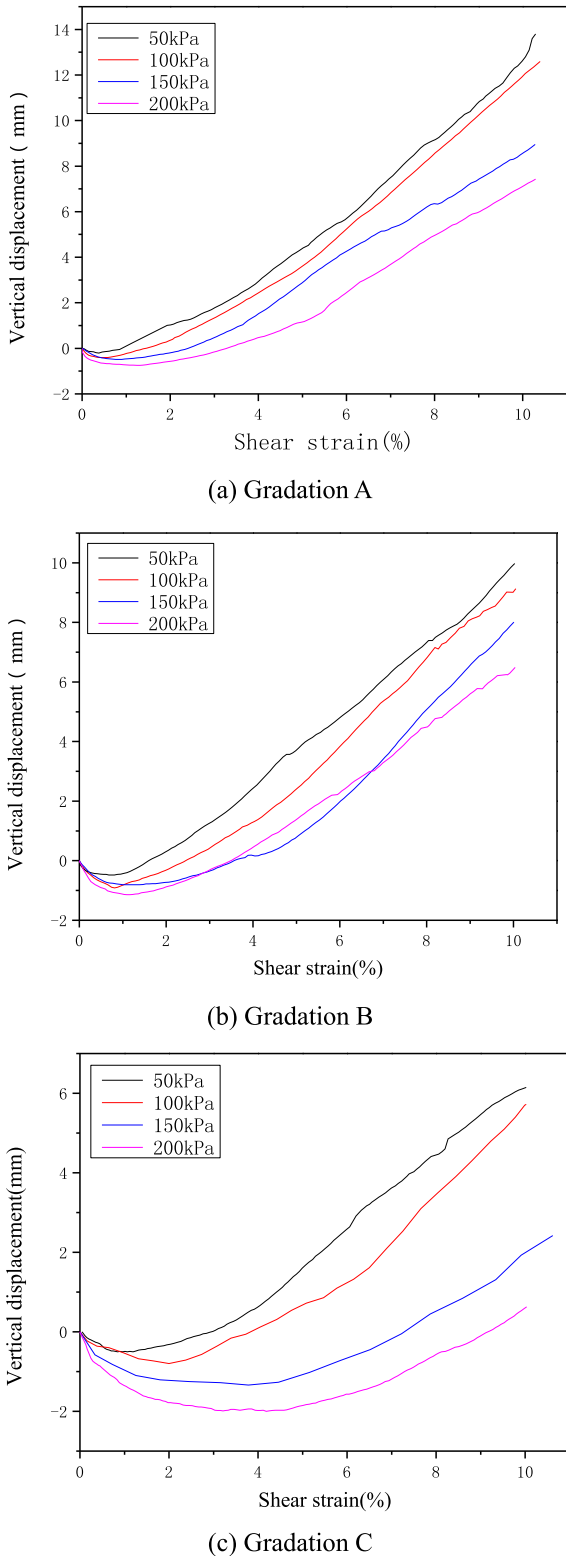


Fig. 6. Shear strain-vertical displacement plots.

increase of vertical pressure, the larger the amplitude attenuates.

### Deformation characteristics

The shear strain-vertical displacement curve of gravel aggregate with different particle sizes during shearing is plotted in Fig. 6. The aggregate was compressed as vertical displacement was negative, while the positive displacement indicated shear dilatancy. The aggregates showed the characteristics of shear dilation throughout the process of shearing. In the initial stage, each group of aggregate was compressed, and then swelled with shearing. Less vertical pressure resulted in smaller compression deformation and more obvious subsequent dilatancy. The maximum amount of compression with the same vertical pressure increased as the gravel size became larger. The corresponding critical shear strain that distinguished compression from dilatancy also increased. For instance, when the vertical pressure was 200 kPa, the maximum compression of gradation A, B, and C was 0.88 mm, 1.21 mm, and 2.01 mm, respectively, while the critical shear strain was 3.2%, 3.6%, and 9.1%.

### Micro-analysis of the shear process

#### Generation of irregular crushed rock particle

Spheres are often used to present particles in PFC3D, which are not appropriate enough to simulate the irregular crushed rock particle. Clump logic can be used to model the irregular particle by combining many spheres with overlapping into a rigid body where contacts between spheres are ignored (Ferrellec and McDowell, 2012; Thakur et al., 2010). However the density of the polygon clumps are always non-uniform which means the calculation is only approximately accurate and the calculation efficiency is relatively low due to too many overlaps (Lu and McDowell, 2007). In this paper, clump logic was also used to create 4 different shapes with limited overlaps (shown in Fig. 7) to simulate crushed rock based on the principle that the volume and mass density of the clump should be same as the previous spheres, and the mass density of the clump can be calculated according to the following Eq. (2):

$$\rho_{cl} = \frac{V_{cl}}{\sum V_b} \rho_b \tag{2}$$

where:  $\rho_{cl}$  is the mass density of the clump,  $\sum V_b$  is the total volume of all spheres in a clump,  $V_{cl}$  is the volume of the clump,  $\rho_b$  is the density of sphere.

#### Specimen generation

Eleven wall elements were used to simulate a direct shear box of the same size as the laboratory apparatus, including two wing plates. Spheres with radius range of 2.0–3.5 cm were generated following a Gaussian distribution to simulate the crushed rock aggregate with the same density which were all then replaced by clumps. The discrete element model is shown in Fig. 8.

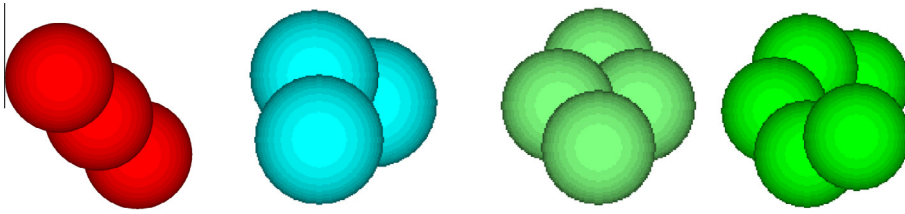


Fig. 7. Clumps.

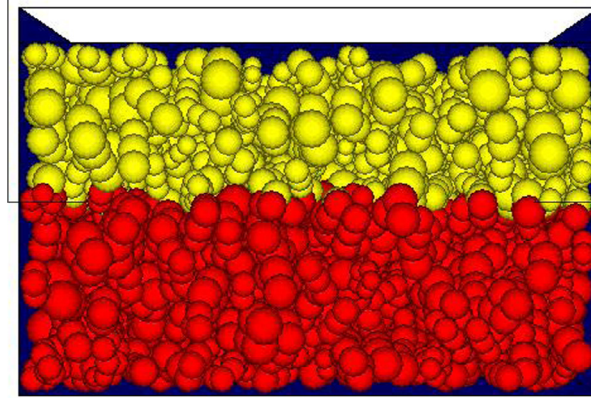


Fig. 8. The discrete element model.

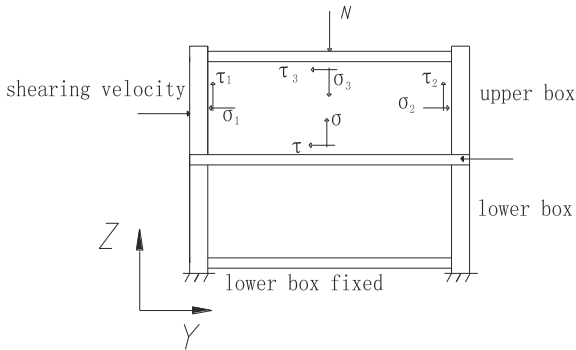


Fig. 9. The internal force of the direct shear box.

Shearing procedure

The servo mechanism was programmed by built-in FISH language in PFC3D. The position of the top wall was adjusted to ensure a constant vertical pressure during shearing. The wall elements composing the upper shear box were pushed at a certain shearing rate. Based on the shear plane stress analysis of Shi et al. (2010) and Indraratna et al. (2014), stress analysis in the Z–Y plane of the three-dimensional discrete element model is shown in Fig. 9.

The normal stress and the shear stress value on the shear plane at any time can be calculated from Eq. (3):

$$\begin{cases} \tau = \sum_{i=1}^n (\tau_{yi} + \sigma_{yi}) / l(b - vt) \\ \sigma = \sum_{i=1}^n (\tau_{zi} + \delta_{zi}) / l(b - vt) \end{cases} \quad (3)$$

where  $i$  is the wall element index and  $n$  is the number of wall elements of the top shear box.  $\tau_{yi}$  and  $\sigma_{yi}$  represent the tangential force and the normal force of different walls in the  $y$  direction on the upper shear box, respectively.  $\tau_{zi}$  and  $\sigma_{zi}$  represent the tangential force and the normal force of different walls in the  $z$  direction on the upper shear box, respectively.  $l$  is the length of the shear box,  $b$  is the width of the shear box, and  $v$  is the shearing velocity. The time step adopted was  $10^{-5}$ /s which could ensure the stability and accuracy of the calculation.

The axial strain and the strain of shearing direction can be calculated according to Eq. (4):

$$\begin{cases} \varepsilon_a = dis_{top\_w} / h \\ \varepsilon_s = vt / b \end{cases} \quad (4)$$

where  $\varepsilon_a$  is the axial strain,  $\varepsilon_s$  is the strain of shearing direction,  $dis_{top\_w}$  is the displacement of the top wall,  $h$  is the height of the sample. All corresponding variables were monitored and recorded during shearing and then output.

The vertical pressure of the numerical model in the direct shear process is shown in Fig. 10. Different vertical pressures overall could be maintained at the target value with only slight fluctuation, which proved that the vertical test conditions met the requirements.

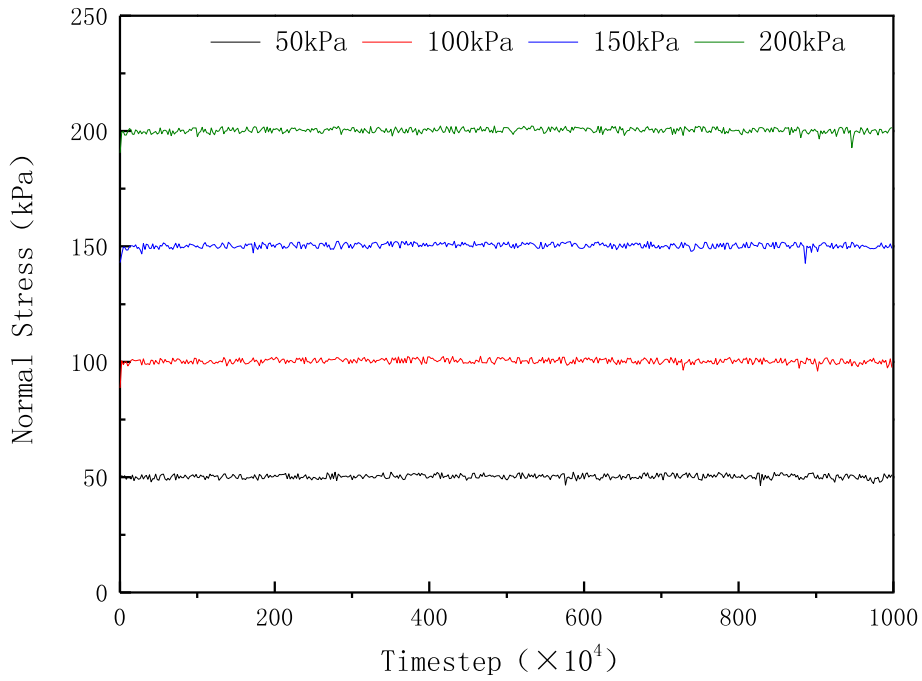


Fig. 10. Vertical stresses of the numerical model during shearing process.

Parameter calibration

The linear contact model was selected for crushed rock as a cohesionless material (Wu and Feng, 2008). The linear model includes the frictional coefficient, normal and

shearing stiffness. Xu et al. (2008) studied the friction of granite by lab test, and the result indicated that the coefficient was about 0.6 which was adopted in this research. Luo et al. (2008) studied the effect of normal and shearing stiffness on the mechanical behavior of granular material, and

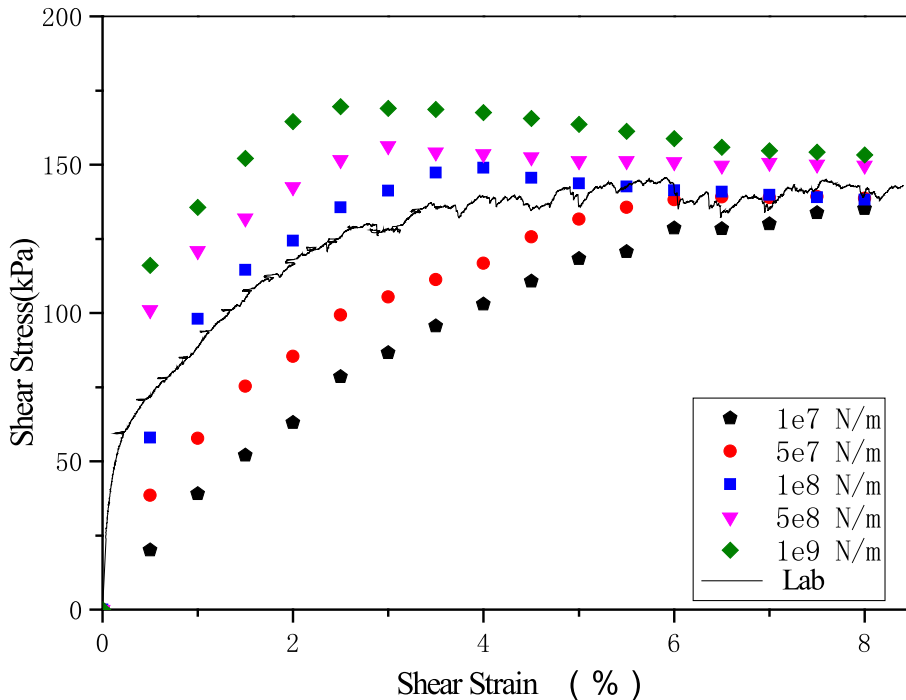


Fig. 11. Shear stress–strain behavior of particle with different stiffness.

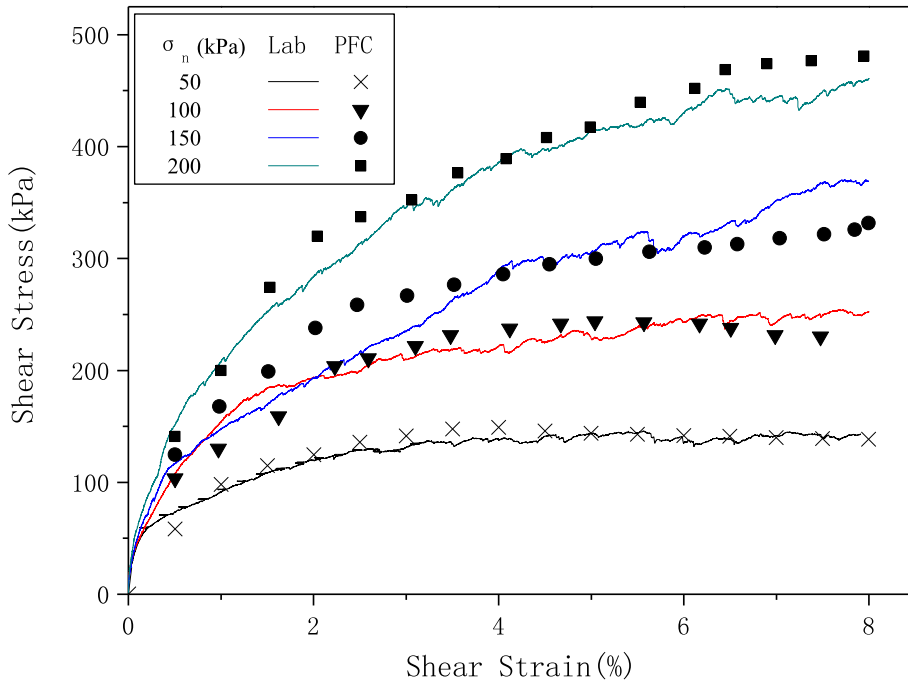


Fig. 12. Comparisons between PFC model and lab tests.

Table 2

Microscopic parameters of the DEM model.

Ball			Wall	
$(k_n)_p$ (N/m)	$(k_s)_p$ (N/m)	$f_p$	$(k_n)_w$ (N/m)	$(k_s)_w$ (N/m)
$1e^8$	$1e^8$	0.6	$1e^9$	$1e^9$

the ratio of normal and shear stiffness are proved to have little influence, according to which the normal and shear stiffness was set to be same in this paper. The normal stiffness of granite ballast was about  $3 \times 10^8$  N/m (Fu et al., 2013), based on which the stiffness of this research was determined. To calibrate the micro parameters, normal stiffness of spheres were set to be  $1 \times 10^7$  N/m,  $5 \times 10^7$  N/m,  $1 \times 10^8$  N/m,  $5 \times 10^8$  N/m,  $1 \times 10^9$  N/m respectively. The

stiffness of the wall was 10 times larger than that of the particle, and the friction coefficient was ignored to simulate the steel box (Indraratna et al., 2014). The shear stress–strain character of lab tests was compared with the numerical results of different particle stiffness as shown in Fig. 11.

The stiffness has a significant influence on the mechanical behavior of the aggregate. The peak shear stress and the initial slope of the curve increase with the stiffness, and the strain of the peak stress shows an opposite trend. The numerical model fits the experimental results best at the stiffness of  $1 \times 10^8$  N/m.

Compare the numerical shear stress–strain curves with the experimental results of different normal stresses to further verify the parameters, and the results were shown in Fig. 12. The numerical results fit well with the experimental results overall, especially at low normal stress.

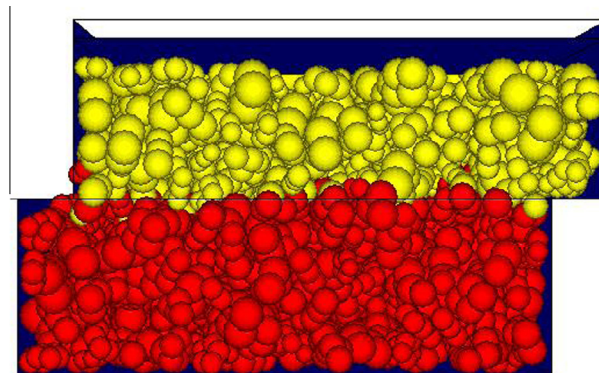


Fig. 13. Post-shearing model.

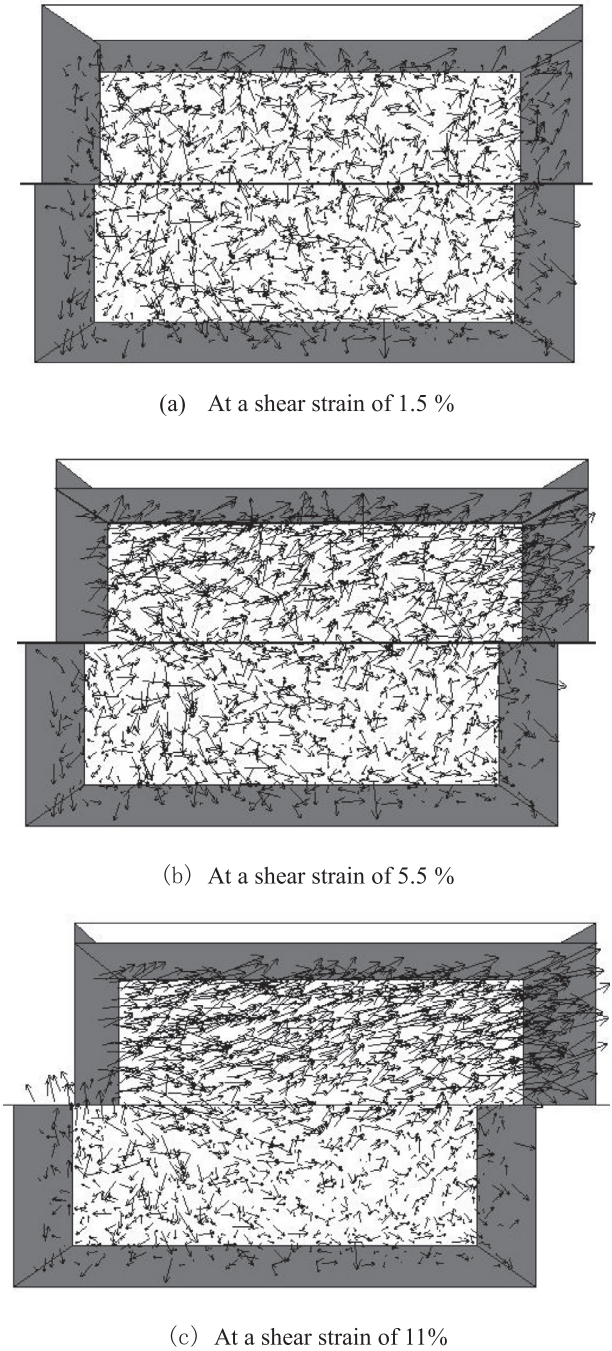


Fig. 14. Displacement vectors of the gravels at the vertical pressure of 50 kPa.

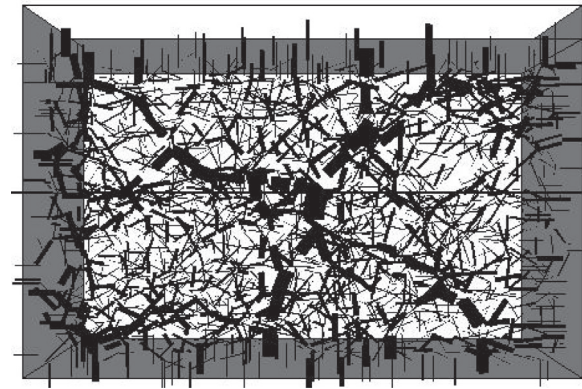
Table 2 shows the final selected parameters, where  $k_n$ ,  $k_s$  represent the normal stiffness and shear stiffness, respectively,  $f$  is the friction coefficient, the subscript of  $p$  represents crushed rock particles, and  $w$  represents the wall.

#### Micro-mechanical analysis

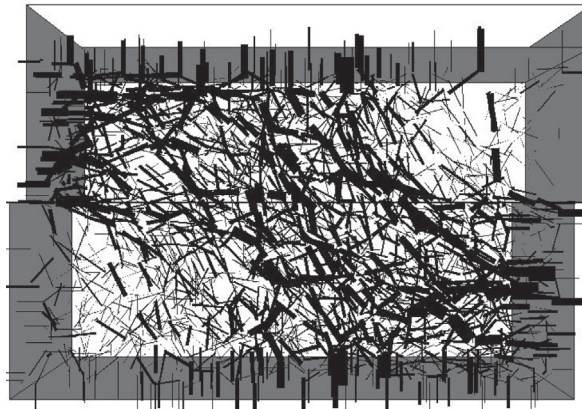
The numerical model after direct shearing was shown in Fig. 13. Compared with Fig. 8, the particles of the shearing surface have obvious dislocation: the particles on the

left and right of the lower box produce upward displacement and the yellow particles on the left of the upper box produce downward displacement.

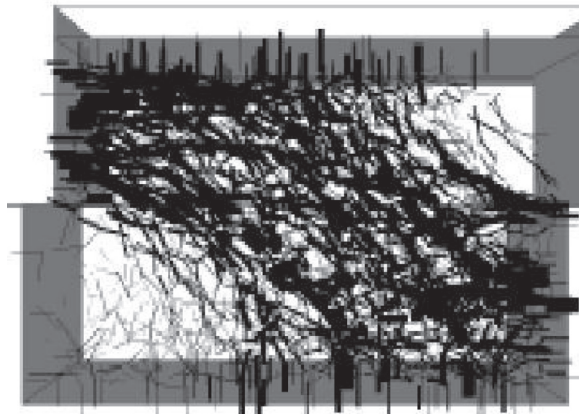
Fig. 14 shows the displacement vectors of different shear strains of 1.5%, 5.5%, and 11% at the vertical pressure of 50 kPa to study the displacement evolution of crushed rock during shearing. The displacement vector of the gravels in the upper box was mainly ultimately stable on the right and top right with the increase of the shear strain, which caused shear dilatancy. The gravels on the left side



(a) Before shearing



(b) At a shear strain of 2%



(c) At a shear strain of 6%

**Fig. 15.** Evolution of distribution of contact stress during shearing with a vertical pressure of 50 kPa.

of the box produced downward displacement and caused corresponding shear contraction.

The displacement of the gravels at the interface of the upper and lower box was more complex with obvious deflection. The volumetric strain of the crushed rock appeared to be inhomogeneous during shearing.

The contact force distribution of different shear strains of 2%, 6% at the vertical pressure of 50 kPa was plotted in Fig. 15, where the thickness of the force chain represents the value of the contact force. The contact force distribution of the shear box was relatively uniform before shearing, transmitting along the vertical direction.

In the figure, the shear band is actually from the upper left of the upper box to the lower right of the lower box with the shearing strain increasing. The crushed rock was more likely to break where the contact force was concentrated.

### Summary and conclusions

Large-scale direct shear tests were conducted to study the mechanical properties of crushed rock aggregates of three different particle sizes with four different vertical pressures, 50 kPa, 100 kPa, 150 kPa, and 200 kPa. The parameters of the numerical model were calibrated and validated by comparing with laboratory test results. Some differences existed between the numerical results and the experimental results due to the shape effect and breakage of the gravel. We analyzed the micro-mechanical characteristics of the aggregates subjected to various direct shear conditions and drew the following main conclusions:

- The shear strength of crushed rock aggregate increased with increasing vertical pressure, and the envelope can be well described by a power function curve.
- The gravel aggregates were compressed in the initial stage of shearing, followed by dilation. Shear contraction was more obvious with the increase of vertical pressure.
- In the selected gravel sizes, the shear strength and the compression of the aggregates increased and the apparent friction angle decreased with the increase of particle size at the same vertical pressure.
- The stiffness can significantly influence the shear behavior of the aggregate, the shear strength and the initial slope of the curve increase with the stiffness, and the strain of the peak stress shows an opposite trend.
- The volumetric strain changes of the aggregate were non-uniform, and principal stress showed obvious deflection during shearing. The orientation of the shear band was mainly from the left of the upper box to the right of the lower box.

### Acknowledgements

This project is supported by the National Natural Science Foundation of China (No. 41371081), the National 973 Project of China (No. 2012CB026104), and the National Natural Science Foundation of China (No. 51378057).

### References

- Cheng G. Permafrost studies in the Qinghai-Tibet plateau for road construction. *J Cold Regions Eng* 2005;19(1):19–29.
- Ferrellec J-F, McDowell GR. Modelling of ballast/geogrid interaction using DEM. *Geosynth Int* 2012;19(6):470–9.
- Fu L, Gong Q, Zhou S, Zou C, Xiao J. Relationships between ballasted track settlement and differential subgrade settlement under train load. *J Vib Shock* 2013;32(14):23–9.
- Goering DJ. Passively cooled railway embankments for use in permafrost areas. *J Cold Regions Eng* 2003;17(3):119–33.
- Goering DJ, Kumar P. Winter-time convection in open-graded embankments. *Cold Reg Sci Technol* 1996;24(1):57–74.
- Indraratna B, Wijewardena LSS, Balasubramaniam AS. Large-scale triaxial testing of grey wacke rockfill. *Géotechnique* 1993;42(01):37–51.
- Indraratna B, Ionescu D, Christie HD. Shear behavior of railway ballast based on large scale triaxial testing. *J Geotech Geoenviron Eng* 1998;124(5):439–49.
- Indraratna B, Ngo N, Rujikiatkamjorn C, Vinod JS. Behavior of fresh and fouled railway ballast subjected to direct shear testing: a discrete element simulation. *Int J Geomech* 2014;14(1):34–44.
- Lai Y, Li J, Niu F, et al. Nonlinear thermal analysis for Qinghai-Tibet railway embankments in cold regions. *J Cold Regions Eng* 2003;17(4):171–84.
- Lai Y, Zhang S, Zhang L, et al. Adjusting temperature distribution under the south and north slopes of embankment in permafrost regions by the ripped-rock revetment. *Cold Reg Sci Technol* 2004;39(1):67–79.
- Lu M, McDowell GR. The importance of modelling ballast particle shape in the discrete element method. *Granular Matter* 2007;12:69–80.
- Luo Yong, Gong Xiao-nan, Lian Feng. Simulation of mechanical behaviors of granular materials by three-dimensional discrete element method based on particle flow code. *Chinese. J Geotech Eng* 2008;30(2):292–7.
- Ma W, Feng GL, Wu QB, et al. Analyses of temperature fields under the embankment with crushed-rock structures along the Qinghai-Tibet railway. *Cold Reg Sci Technol* 2008;53:259–70.
- Mu Y, Ma W, Sun Z, Liu Y. Comparative analysis of cooling effect of crushed rock embankment along the Qinghai-Tibet railway. *Rock Soil Mech* 2010;31(S1):284–92.
- Saboundjian S, Goering DJ. Air convection embankment for roadways: field experimental study in Alaska. *Transport Res Rec: J Transport Res Board* 2003;1821(1):20–8.
- Shao L, Chi S, Zhang Y, Tao J. Study of triaxial shear tests for rockfill based on particle flow code. *Rock Soil Mech* 2013;34(03):711–20.
- Shi D, Zhou J, Liu W, Deng Y. Exploring macro- and micro-scale responses of sand in direct shear tests by numerical simulations using non-circular particles. *Chin J Geotech Eng* 2010;32(10):1557–65.
- Thakur PK, Vinod JS, Indraratna B. Effect of particle breakage on cyclic densification of ballast: a DEM approach. *Proc IOP Conf Series: Mater Sci Eng* 2010:122–9.
- Tian K, Zhang H, Luo Y. Shear strength and stress-strain properties of rockfill materials. *Chin J Rock Mech Eng* 2005;24(04):657–61.
- Wee LL. *Mechanics of railway ballast behavior*. Nottingham, UK: The University of Nottingham; 2004. 5.
- Wu J, Feng X. Particle flow simulation of soil under high-speed shear. *Chin J Rock Mech Eng* 2008;27(S1):3064–9.
- Wu Q, Zhao S, Ma Wei, et al. Monitoring and analysis of cooling effect of block stone embankment for Qinghai-Tibet Railway. *Chin J Geotech Eng* 2005;12:1386–90.
- Xu Qiongping, Wang Detong, Lu Yusheng. Experimental study on static friction coefficient of granite survey. *J PLA Univ Sci Technol* 2008;09(03):270–3.
- Zhou J, Jia M. *Meso-scale model tests and numerical simulation in geotechnique*. Beijing: Science Press; 2008.